Petroleum Science 23 (2026) 5788–5799

Contents lists available at ScienceDirect

Petroleum Science

journal homepage: www.keaipublishing.com/en/journals/petroleum-science

Original Paper

Unlocking residual oil after CO_2 flooding: The role of tributyl citrate as a solvent-based mobilizing agent

Zhi-Hao Zhang [a,b], Ming-Wei Zhao [a,b,*], Zhong-Zheng Xu [a,b], Qin-Fang Ding [c], Yu-Xin Xie [a,b], Ying-Nan Wang [a,b], Yi-Zheng Zhang [a,b], Huan Zhang [a,b], Xu-Guang Song [d]

[a] State Key Laboratory of Deep Oil and Gas, China University of Petroleum (East China), Qingdao, 266580, Shandong, China
[b] Key Laboratory of Unconventional Oil & Gas Development, China University of Petroleum (East China), Ministry of Education, Qingdao, 266580, Shandong, China
[c] School of Petroleum and Chemical Engineering, Dongying Vocational College, Dongying, 257091, Shandong, China
[d] Department of Chemical and Materials Engineering, University of Alberta, Edmonton AB T6G 1H9, Canada

ARTICLE INFO

Article history:
Received 25 February 2026
Received in revised form
15 June 2026
Accepted 17 June 2026
Available online 22 June 2026

Edited by Yan-Hua Sun

Keywords:
Tributyl citrate
Residual oil
CO_2 flooding
Asphaltene/resin deposition
Solvent effect

ABSTRACT

CO_2 flooding in light-oil reservoirs can induce compositional redistribution and heavy-fraction deposition, leading to pore-structure deterioration, permeability reduction, and limited oil recovery. Although tributyl citrate (TBC) is a promising solvent-type additive for improving oil fluidity and CO_2–oil compatibility, its role in remobilizing residual oil affected by deposition remains insufficiently understood. This study integrates visual interfacial observations and PVT measurements with core-flooding tests and multiscale characterization to elucidate CO_2–oil interaction-driven deposition and the TBC-assisted remobilization process. Results show that CO_2 preferentially extracts light hydrocarbons (C_1–C_9) while enriching intermediate (C_{10}–C_{29}) and heavy components (C_{30+}), thereby destabilizing crude-oil colloidal structures and promoting irreversible deposition. In homogeneous cores, miscible CO_2 flooding at 20 MPa achieves a high recovery of 77.08% but also induces 15.28% heavy-component deposition and up to 38.23% permeability reduction. In contrast, fractured cores exhibit less deposition but markedly lower sweep efficiency. The addition of TBC mitigates these adverse effects by suppressing viscosity growth, enhancing CO_2 solubility and oil swelling, and improving CO_2–oil compatibility. These synergistic effects strengthen interfacial mass transfer and provide an additional 13%–18% recovery enhancement beyond CO_2 flooding alone. Multiscale observations suggest that TBC reduces the aggregation tendency of deposited heavy components and improves pore-scale flow continuity. These findings provide insight into the remobilization of deposition-affected residual oil after CO_2 flooding and demonstrate the potential of TBC to mitigate formation damage and enhance CO_2-EOR performance in light-oil reservoirs.

1. Introduction

CO_2 flooding has been widely recognized as one of the most promising technologies for enhanced oil recovery (EOR) and carbon capture, utilization, and storage (CCUS), playing a crucial role in achieving global carbon neutrality goals (Hu et al., 2019; Jiang and Ashworth, 2021; Wang et al., 2023). Through mechanisms such as oil swelling, viscosity reduction, and interfacial tension minimization, CO_2 injection significantly improves microscopic displacement efficiency in both mature and low-permeability reservoirs (Holm and Josendal, 1974; Kumar et al., 2022; Martin and Taber, 1992). Nevertheless, both field practice and laboratory studies have demonstrated that CO_2 flooding can also induce the precipitation of asphaltene and resin fractions, resulting in pore blockage, reduced permeability, and decreased recovery efficiency (Alizadeh et al., 2011; Cheshkova et al., 2019).

This behavior is closely related to CO_2–oil mass transfer and compositional redistribution during contact. Within the oil phase, light hydrocarbons can be extracted into the CO_2-rich phase, while intermediate components undergo redistribution and relative enrichment in the residual oil, continuously depleting stabilizing

* Corresponding author.
E-mail address: zhaomingwei@upc.edu.cn (M.-W. Zhao).

Peer review under the responsibility of China University of Petroleum (Beijing).

https://doi.org/10.1016/j.petsci.2026.06.033
1995-8226/

species and promoting asphaltene–resin aggregation (Choiri and Hamouda, 2011; Mousavi et al., 2016; Zuo et al., 2023). Such deposition not only increases the viscosity of the retained oil but may also alter pore-throat connectivity and fluid flow behavior, thereby aggravating formation damage (Ding et al., 2013; Huang et al., 2022; Li et al., 2021b). Notably, CO_2 can induce substantial asphaltene and resin precipitation even in light oils with low asphaltene content (Sarma, 2003).

CO_2-induced precipitation of asphaltenes and resins enriches the retained oil in polar heavy fractions, which increases viscosity and reduces mobility (Li et al., 2020; Yu et al., 2022; Zhao et al., 2025). Consequently, recovering this deposition-affected residual oil becomes challenging. Conventional approaches mainly include physical methods (e.g., thermal recovery and dilution) and additive-assisted methods (e.g., surfactant-based agents, solvent-type additives, and polymeric dispersants) (El-Hoshoudy et al., 2021; Yuan et al., 2018). Although physical methods can temporarily reduce oil viscosity, they are energy-intensive, costly, and generally unsuitable for CO_2-flooding environments. In contrast, additive-assisted methods have emerged as an efficient and economical alternative (Hou et al., 2019; Ke et al., 2018; Mehrabianfar et al., 2021; Wang et al., 2016; Zhong et al., 2021). Among them, surfactant-based agents mainly improve displacement by regulating interfacial properties, whereas solvent-type additives primarily enhance solvation and colloidal stability, thereby weakening intermolecular associations and suppressing heavy-component re-aggregation (Chen et al., 2023; Jia et al., 2020). Because CO_2 flooding in light oils mainly causes compositional redistribution and destabilization of heavy organic fractions. Thus, solvent-type additives are particularly relevant for remobilizing deposition-affected residual oil by restoring solvation and suppressing re-aggregation.

Tributyl citrate (TBC) has recently attracted attention as a potential solvent-type additive because of its mixed polar–nonpolar molecular structure, compatibility with crude oil and CO_2, and favorable environmental properties (Bao et al., 2023; Cao, 2023; Cao and Li, 2022; Gao et al., 2023; Yuan et al., 2024). Previous studies have shown that TBC can enhance CO_2 solubility and modify the phase behavior and fluid properties of crude oil systems (Al-Azani et al., 2020, 2021; Xue et al., 2024). These features suggest that TBC may help alleviate deposition-related flow impairment during CO_2 flooding. However, current understanding of TBC in CO_2–oil systems remains limited. Most previous studies have focused on its bulk-phase effects, such as viscosity modification or miscibility enhancement, while its role in the coupled processes of compositional redistribution, organic deposition, and residual-oil remobilization has received much less attention.

This issue is particularly important for light crude oils, whose molecular composition, phase behavior, and CO_2 solubility differ markedly from those of heavy oils (Li et al., 2021a; Wei et al., 2020). As a result, the mechanisms controlling deposition formation and post-deposition remobilization in light oil systems may also be distinct. A clearer understanding of how TBC influences these coupled processes is therefore essential for improving CO_2-EOR performance and mitigating formation damage in light oil reservoirs (Shen and Sheng, 2018; Zhang et al., 2022).

As a result, this study investigates the CO_2-induced deposition of heavy fractions and the TBC-assisted mobilization of residual oil in light oil reservoirs. Through a combination of visual PVT experiments, core-scale CO_2 flooding tests, and microscopic characterization techniques—including nuclear magnetic resonance (NMR), scanning electron microscopy (SEM), and atomic force microscopy (AFM)—this study elucidates the coupled effects of CO_2–oil interactions, deposition behavior, and additive regulation. The findings provide new insights into the mechanisms governing heavy-component mobilization and offer a scientific basis for mitigating CO_2-induced formation damage and improving recovery efficiency in light oil reservoirs.

2. Experimental section

2.1. Materials

The cores and crude oil used in this study were collected from a representative block of the Changqing Oilfield. The basic parameters of the core samples are listed in Table 1. The crude oil has a viscosity of 7.79 mPa·s and a density of 0.835 g/cm^3 at room temperature. It contains 1.62 wt% resins and 0.57 wt% asphaltenes. The carbon number distribution of the crude oil, determined by gas chromatography, is shown in Table 2, indicating that the oil is dominated by light and mid-range components, which is characteristic of light crude oil. TBC was purchased from Macklin Biochemical Co., Ltd. CO_2 with a purity of 99.9% was supplied by Yantai Deyi Gas Co., Ltd. The *n*-heptane and toluene were provided by the China National Pharmaceutical Group Corporation (Sinopharm). All chemicals were used as received without further purification.

2.2. Experimental methods

2.2.1. Measurements of the MMP

The minimum miscibility pressure (MMP) between CO_2 and crude oil was determined using the interfacial tension disappearance method (Yang et al., 2019). Experiments were performed with a high-temperature and high-pressure interfacial tensiometer (Fig. 1(a)) at 55, 65, and 75 °C, respectively. During each test, the crude oil droplet was formed within the high-pressure chamber, and CO_2 was incrementally injected to reach a series of target pressures. At each equilibrium state, the interfacial tension (IFT) between CO_2 and crude oil was recorded. The IFT–pressure data were then linearly extrapolated to zero, and the corresponding pressure was identified as the MMP.

2.2.2. CO_2–oil interaction experiments

CO_2–oil interaction experiments were conducted in a high-pressure visual PVT cell (Fig. 1(b)) to examine the compositional evolution and deposition of heavy components under CO_2 exposure. For each experiment, the entire system was thoroughly

Table 1
Core sample parameters.

Number	Core type	Length, cm	Diameter, cm	Permeability, mD	Porosity, %
1	Homogeneous core	6.80	2.50	8.78	14.83
2		7.06	2.55	8.43	10.99
3		7.13	2.53	8.01	10.86
4	Fractured core	7.05	2.45	9.57	11.63
5		7.00	2.48	9.65	11.43
6		7.04	2.55	9.32	10.57

Table 2
Compositional analysis of the oil sample used.

Component	Stabilized condensate, mol%	Component	Stabilized condensate, mol%	Component	Stabilized condensate, mol%
$\leq C_6$	0.99	C_{15}	3.27	C_{24}	2.20
C_7	4.81	C_{16}	2.80	C_{25}	2.51
C_8	3.69	C_{17}	3.29	C_{26}	2.52
C_9	3.14	C_{18}	3.08	C_{27}	2.75
C_{10}	3.13	C_{19}	2.76	C_{28}	2.62
C_{11}	2.88	C_{20}	2.73	C_{29}	2.40
C_{12}	2.91	C_{21}	2.52	C_{30+}	31.35
C_{13}	3.13	C_{22}	2.60		
C_{14}	3.71	C_{23}	2.20		

cleaned, dried, and purged with nitrogen to ensure cleanliness and airtight sealing. A measured amount of crude oil was injected into the cell, after which CO_2 was introduced to reach the designated pressure. The temperature was maintained at 75 °C, and the mixture was intermittently stirred for 12 h to promote mass transfer and achieve phase equilibrium.

Following equilibration, oil samples were collected and analyzed to determine the contents of saturates, aromatics, resins, and asphaltenes (SARA fractions), as well as the carbon number distribution. These analyses were used to characterize CO_2-induced extraction behavior and heavy-component precipitation, and to quantify the degree of deposition during CO_2 exposure. To ensure data reliability, the SARA analyses were performed on repeated samples, and the average values were used for analysis.

2.2.3. Physical parameters of the crude oil

The changes in crude oil physical parameters after CO_2 dissolution and TBC addition were examined using a high-pressure visual PVT cell (Fig. 1(b)). Before each experiment, the PVT cell and connecting lines were thoroughly cleaned, dried, and purged with nitrogen. A mixture of crude oil and a predetermined amount of TBC was injected into the cell, followed by CO_2 injection until the system pressure reached 20 MPa. The temperature was maintained at 75 °C to simulate reservoir conditions.

At 75 °C, constant composition expansion experiments were performed to determine the bubble-point pressure and assess the volumetric expansion behavior of the oil–CO_2–TBC system during depressurization. The bubble point was identified as the transition from a single-phase liquid to a gas–liquid two-phase state. After equilibrium was established, stepwise degassing tests were conducted to release dissolved CO_2 and to record changes in oil volume and density. The resulting PVT data were used to evaluate the effects of TBC on CO_2 solubility, oil swelling, and phase-transition behavior, thereby elucidating its role in improving the fluidity and compositional stability of light crude oil.

2.2.4. Microscopic deposition morphology scanning of heavy components

The microscopic deposition morphology of heavy components after CO_2 exposure was analyzed using AFM. An NCHV probe was used, and the scanning area was set to 40 μm × 40 μm. Following the CO_2–oil interaction, asphaltene–resin aggregates were separated from the oil phase using the standard *n*-heptane precipitation method. A measured amount of the extracted heavy components was dissolved in 20 mL of toluene and left to stand for 24 h to ensure complete dissolution. The resulting solution was then spin-coated onto a clean glass substrate to form a uniform thin film, followed by nitrogen drying to remove residual solvent.

The prepared samples were examined in tapping mode to characterize the surface morphology and aggregation behavior of the heavy components. To improve statistical reliability, each sample was analyzed at multiple independently selected regions under the same scanning conditions. The characteristic surface parameters were statistically evaluated. The reported values were expressed as average values with standard deviations. The AFM images were used to provide detailed information on the size, distribution, and three-dimensional microstructure of the deposits, enabling microscopic evaluation of CO_2-induced heavy-component aggregation and deposition.

2.2.5. Core flooding experiments

Core flooding experiments were conducted to evaluate the effect of TBC on the mobilization of residual oil after CO_2 flooding (Fig. 1(c)). Natural sandstone cores were cleaned, dried at 105 °C for 72 h, and then measured for porosity and permeability. For fractured-core experiments, artificial fractures were created in selected sandstone cores using the Brazilian splitting method (Bian et al., 2022; Guo et al., 2024). Specifically, diametrical compressive loading was applied to the core until tensile failure occurred, generating a single longitudinal fracture along the core axis. The induced fracture had an aperture of approximately 0.05 mm and served as a preferential flow path during the subsequent flooding experiments. All cores were then vacuum-saturated with crude oil for 48 h to ensure complete saturation, followed by NMR characterization to obtain the initial pore-structure distribution. Before the flooding experiments, the fractured cores were reassembled, wrapped with a heat-shrink sleeve, and mounted in the core holder under confining pressure. The cores were subsequently stabilized at 75 °C to simulate reservoir conditions.

CO_2 flooding was carried out at an injection rate of 0.1 mL/min until no further oil production was observed at the outlet. Throughout the process, the injection pressure, oil production volume, and differential pressure were continuously monitored. After CO_2 flooding, NMR scanning was performed to quantify the distribution of residual oil and the extent of heavy-component deposition.

Following primary CO_2 flooding, 0.5 pore volumes (PV) of pure TBC were injected into the core as a post-flooding solvent slug. The core was subsequently shut in for 1 h to ensure sufficient contact between TBC and the residual crude oil. Thereafter, secondary CO_2 flooding was conducted under the same temperature, pressure, and flow rate. The contents of heavy components (asphaltenes and resins) were determined according to the NB/SH/T 0509–2010 standard (test method for separation of asphalt into four fractions), and the heavy-component deposition rate was calculated using Eq. (1):

$$w = \frac{m_a - m_b}{m_a} \times 100\% \tag{1}$$

where m_a represents the total mass of asphaltenes and resins entering the core, and m_b represents the mass recovered in the effluent oil.

The heavy-component deposition rate defined by Eq. (1) represents the retained fraction of asphaltenes and resins relative to

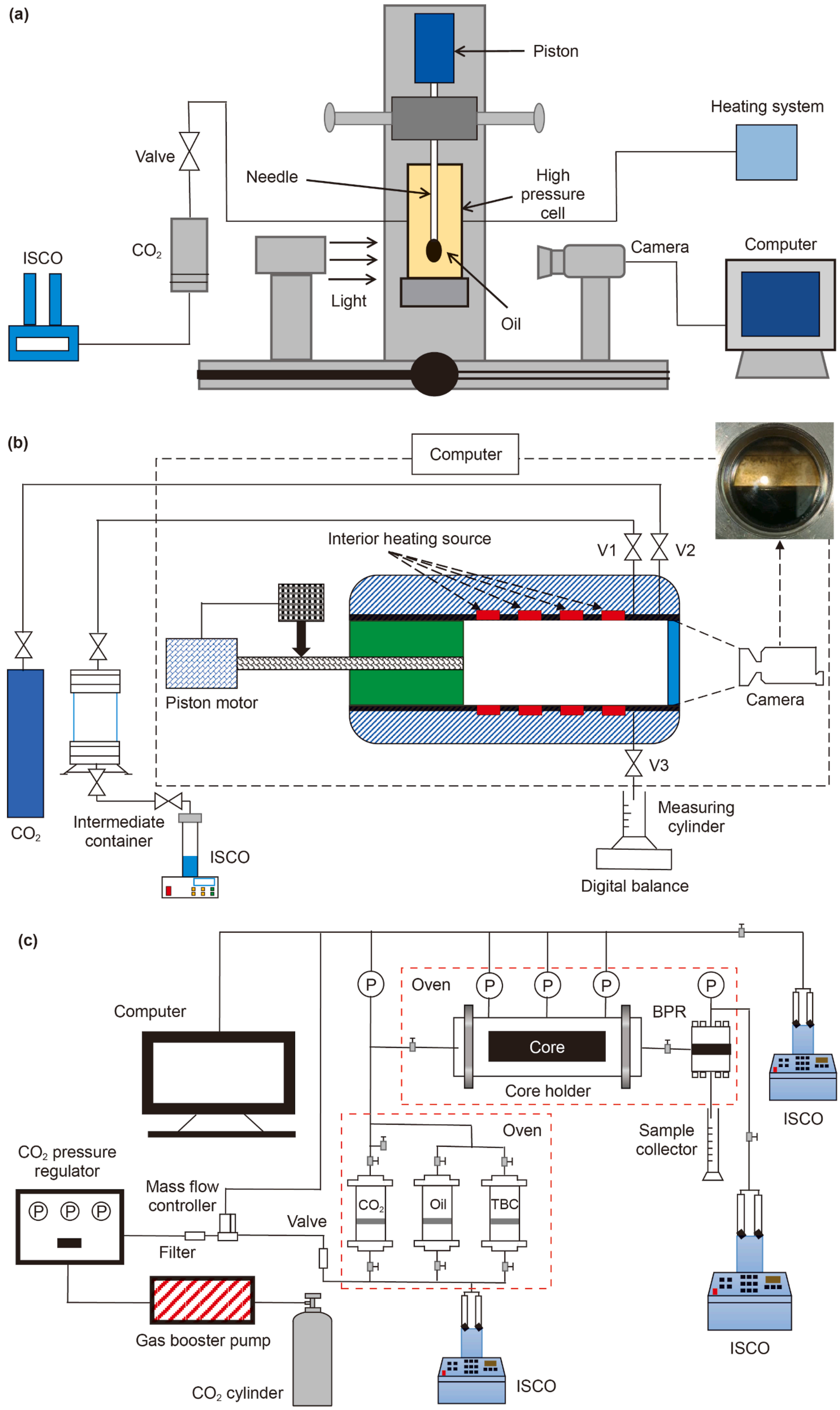

Fig. 1. Experimental apparatus used to evaluate the effect of TBC on CO_2–oil system: (**a**) high-pressure pendant-drop interfacial tensiometer; (**b**) visual PVT apparatus; (**c**) experimental apparatus for CO_2 flooding.

the total mass entering the core. In addition, the porosity damage rate and permeability damage rate in this work are expressed as the relative reductions after flooding with respect to the initial porosity and permeability, respectively. Each deposition measurement was repeated, and the average value was used for subsequent analysis.

3. Results and discussion

3.1. Equilibrium IFT and MMP

A lower MMP indicates stronger CO_2–oil miscibility and a greater ability of CO_2 to extract light and intermediate hydrocarbons from crude oil (Lashkarbolooki and Ayatollahi, 2018). MMP can be evaluated by several experimental methods, including slim-tube, rising-bubble, multiple-contact, and vanishing interfacial tension (VIT/IFT) tests. Among these, the slim-tube test is generally regarded as the most representative method for multi-contact miscibility in porous media, whereas the VIT/IFT method is more efficient for laboratory screening and requires less experimental time. However, the MMP estimated from IFT extrapolation may be influenced by the selected pressure range, the extrapolation procedure, and the compositional complexity of the CO_2–oil system. Therefore, in this study, the equilibrium IFT between CO_2 and light crude oil was measured using a high-temperature and high-pressure interfacial tensiometer over a series of pressures at fixed temperatures, and the IFT–pressure relationship was extrapolated to zero to obtain an experimentally supported estimate of MMP.

As illustrated in Fig. 2, the IFT decreases with increasing pressure, indicating progressive dissolution of CO_2 into the oil phase and a gradual approach to miscibility. At lower pressures, the oil droplet maintains a distinct and well-defined interface, whereas near the miscibility condition the boundary becomes blurred and a fog-like CO_2 phase appears around the droplet. These visual changes reflect the evolution of the CO_2–oil system as it transitions toward the miscible state. Linear extrapolation of the IFT–pressure relationship yields an MMP of 18.03 MPa at 75 °C.

A pronounced temperature dependence was observed. As temperature increases, CO_2 solubility in the oil phase decreases, resulting in higher MMP values. Specifically, the measured MMPs were 14.01 MPa at 55 °C, 16.14 MPa at 65 °C, and 18.03 MPa at 75 °C. These results confirm that lower temperatures facilitate miscibility by promoting CO_2 dissolution and improving CO_2–oil interactions.

3.2. CO_2–oil interactions

The interaction between CO_2 and crude oil plays a decisive role in controlling miscibility behavior and heavy-component deposition during CO_2 flooding. In this study, the CO_2–oil interface was visualized under reservoir conditions (75 °C, 20 MPa) using a high-pressure PVT system to examine compositional redistribution and phase evolution. Crude-oil samples collected before and after CO_2 exposure were analyzed for SARA fractions and carbon number distribution to quantify extraction and aggregation behavior.

As shown in Fig. 3(a), when crude oil is exposed to CO_2, the oil phase undergoes noticeable volumetric expansion, indicating enhanced mass transfer and component exchange. With prolonged CO_2 exposure, black particulates gradually appear in the oil phase, indicating heavy-component deposition. Quantitative compositional analysis (Fig. 3(b) and (c)) reveals that after CO_2 dissolution, light components (C_{10} and below) decrease by 6.96%, heavy components (C_{30+}) increase by 3.40%, and intermediate fractions (C_{10}–C_{29}) exhibit a relative increase, reflecting redistribution within the oil phase. These results indicate that CO_2 extracts light hydrocarbons and destabilizes the asphaltene–resin network, thereby promoting heavy-component aggregation.

To further elucidate the microscopic process of compositional redistribution during CO_2–oil contact, the molecular-interaction mechanism is illustrated in Fig. 4. CO_2 molecules preferentially dissolve into the oil phase and interact with light hydrocarbons, promoting their extraction and vaporization. As contact proceeds, intermediate components (C_{10}–C_{29}) undergo chain stretching and rearrangement, enhancing their interaction with CO_2 and facilitating gradual stripping into the gas phase (Seyyedsar et al., 2016; Rezk and Foroozesh, 2019). In contrast, heavy components such as asphaltenes and resins, dominated by strong self-association and polar interactions, resist CO_2 penetration and tend to aggregate.

This extraction process results in a distinct compositional redistribution. Light components are continuously removed, while intermediate components become elongated and dispersed. Meanwhile, heavy components may aggregate through a combination of interactions, including π–π interactions between aromatic moieties, hydrogen bonding/acid–base interactions involving heteroatoms, as well as other polar and van der Waals interactions (Tan et al., 2023). The imbalance among these processes governs heavy-component deposition and the formation of viscous network structures within the oil phase, providing a molecular-level explanation for the experimentally observed compositional evolution during CO_2 flooding (Zuo et al., 2023).

3.3. CO_2 flooding performance and heavy-component deposition

Core-flooding experiments were conducted on both homogeneous and fractured sandstone cores at various injection pressures during CO_2 flooding. The analysis was guided by the MMP

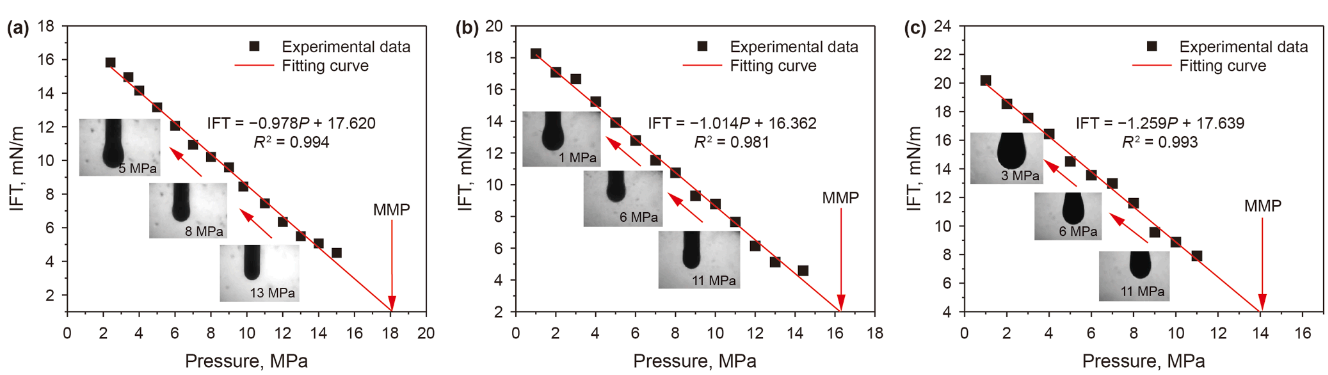

Fig. 2. Equilibrium IFT and MMP of the CO_2–oil system at different temperatures: (**a**) 75 °C; (**b**) 65 °C; (**c**) 55 °C.

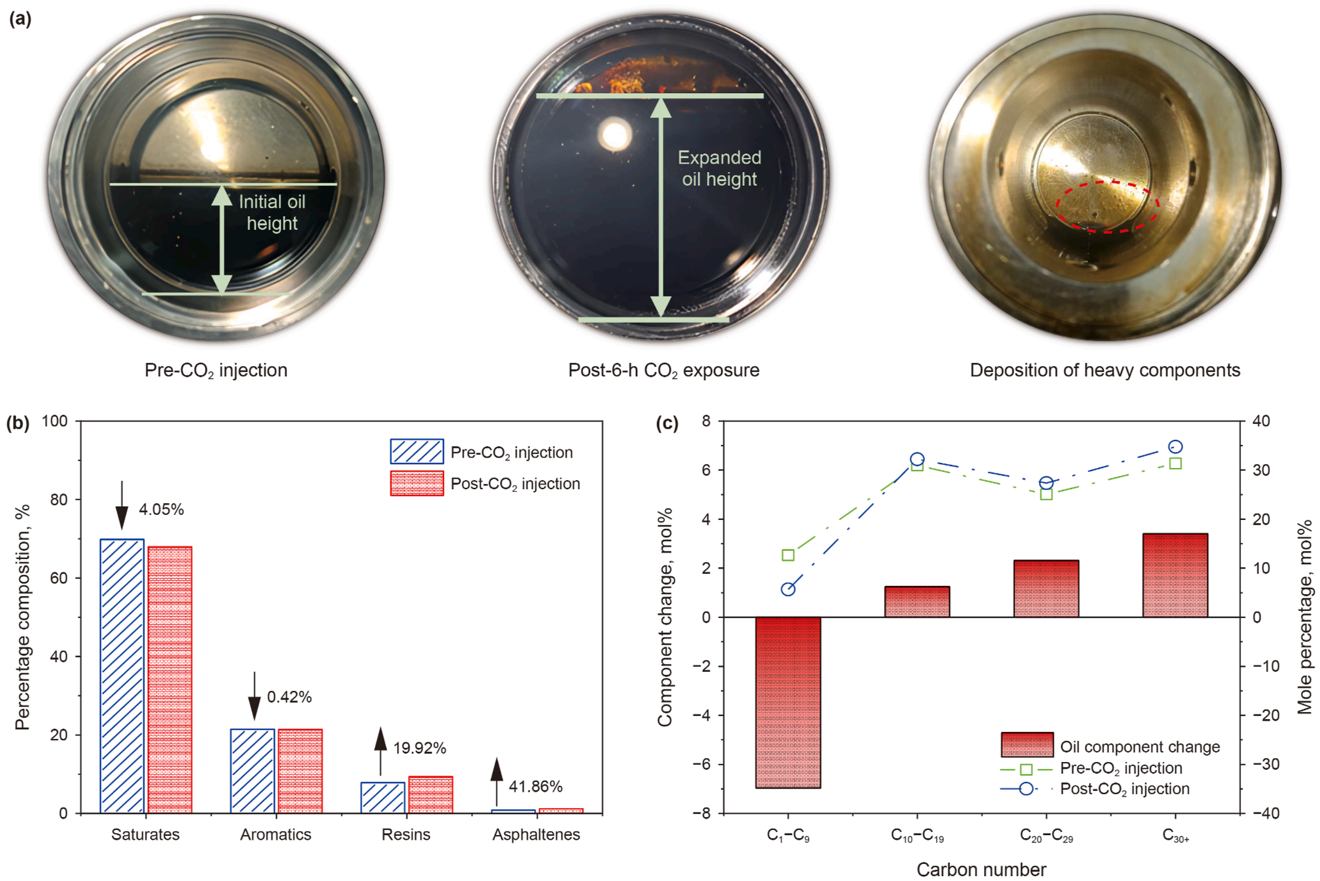

Fig. 3. Compositional evolution and heavy-component deposition in crude oil pre- and post-CO_2 exposure: (**a**) heavy-component deposition; (**b**) SARA fractions; (**c**) carbon number distribution (pre- and post-CO_2 injection) and component changes.

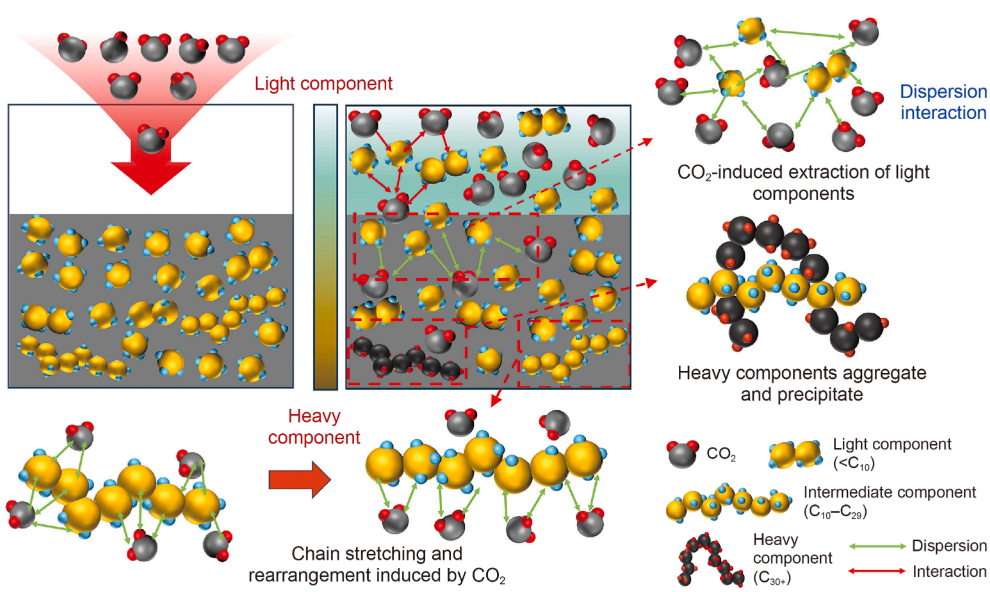

Fig. 4. Schematic diagram of molecular interactions in the CO_2–oil system during CO_2 exposure.

determination and PVT results to evaluate the relationship between oil recovery and heavy-component deposition.

As shown in Fig. 5(a), in homogeneous cores, both recovery and heavy-component deposition increase with injection pressure. With the pressure increasing, recovery improves markedly, from 39.41% at 14 MPa to 68.65% at 18 MPa and 77.08% at 20 MPa, respectively, while heavy-component deposition increases from 7.37% to 13.97% and 15.28%. This trend indicates that higher-

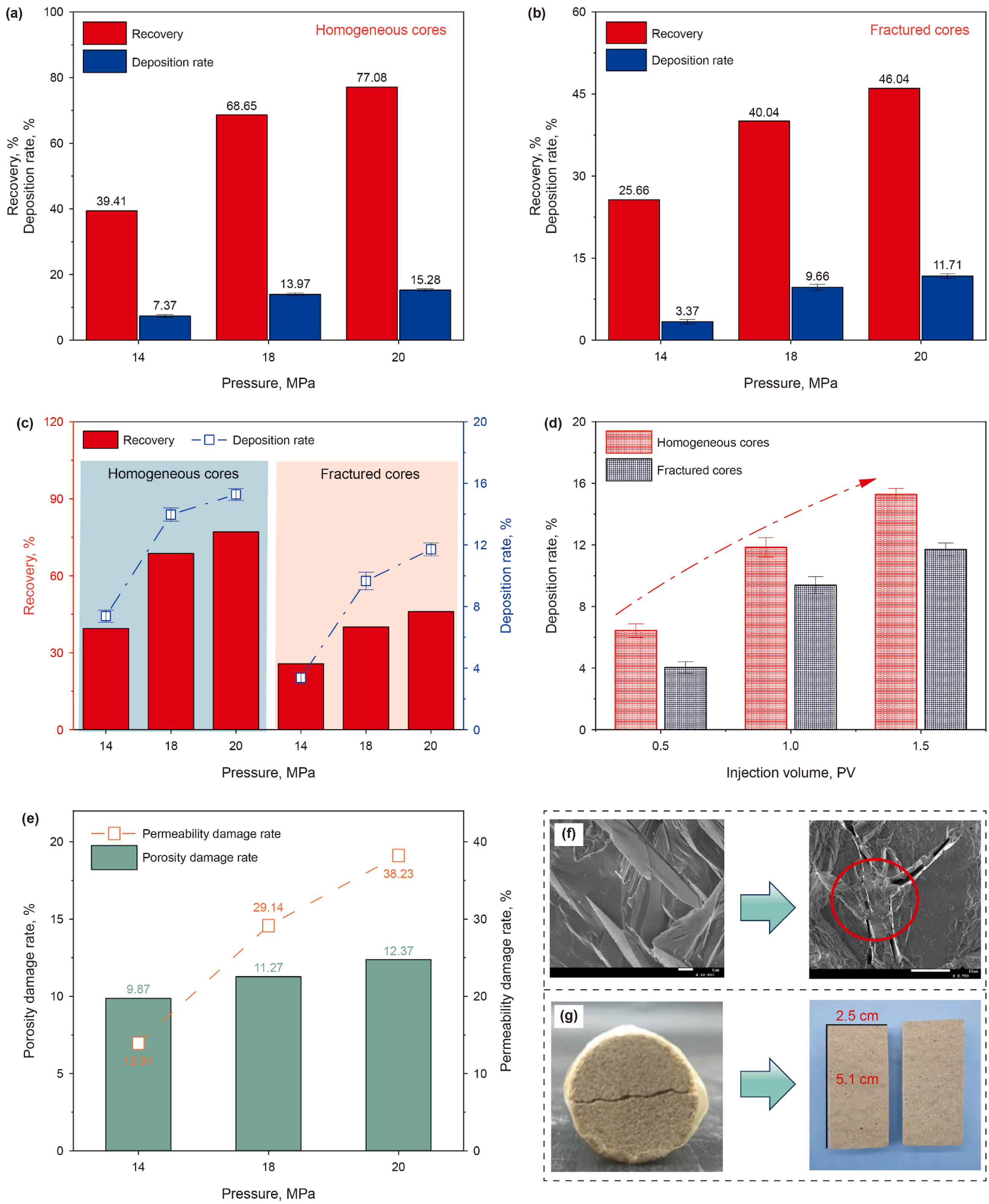

Fig. 5. CO_2 flooding performance and heavy-component deposition in both homogeneous and fractured cores: (**a**, **b**) ultimate recovery and heavy-component deposition in homogeneous and fractured cores at different pressures; (**c**) direct comparison of recovery and heavy-component deposition between homogeneous and fractured cores at different pressures; (**d**) dynamic evolution of heavy-component deposition with injection volume in homogeneous and fractured cores at 20 MPa; (**e**) porosity damage and permeability damage rates at different pressures in homogeneous cores; (**f**) SEM images showing heavy-component deposition on homogeneous-core surfaces; (**g**) fractured core samples.

pressure CO_2 flooding not only improves displacement efficiency but also intensifies compositional redistribution and the deposition of heavy fractions.

In fractured cores (Fig. 5(b) and (g)), the oil recovery increases with pressure, reaching 25.66%, 40.04%, and 46.04% at 14, 18, and 20 MPa, respectively. However, the corresponding heavy-component deposition remains consistently lower than that in homogeneous cores, at 3.37%, 9.66%, and 11.71%. This reduced deposition is attributed to gas channeling through fractures, which causes early breakthrough and matrix bypassing, thereby weakening effective CO_2–oil contact and reducing the extraction intensity responsible for heavy-component accumulation.

The contrast between the two types of cores is more clearly illustrated in Fig. 5(c). At the same pressure, fractured cores consistently exhibit both lower recovery and reduced heavy-component deposition compared to homogeneous cores. For example, at 20 MPa, the recovery decreases from 77.08% in the homogeneous core to 46.04% in the fractured core, while the corresponding heavy-component deposition decreases from 15.28% to 11.71%. Similar trends are observed at 14 and 18 MPa. These quantitative differences indicate that the lower heavy-component deposition in fractured cores does not reflect a more favorable displacement process. Instead, it is mainly attributable to fracture-induced preferential flow and the associated reduction in effective CO_2–oil contact time and contact volume within the matrix. As a result, the buildup of deposited heavy components is suppressed, but the sweep efficiency of the matrix is also significantly reduced.

To further illustrate the dynamic differences in deposition behavior, Fig. 5(d) presents the cumulative heavy-component deposition at 20 MPa as a representative miscible condition. In both core types, deposition increases with injection volume. However, the deposition in fractured cores remains lower throughout the flooding process than that in homogeneous cores. This result confirms that fracture-induced channeling weakens CO_2–oil contact and suppresses the progressive buildup of deposited heavy components in the matrix.

Reservoir property analysis (Fig. 5(e)) shows that the porosity damage rate increases slightly, from 9.87% to 12.37%, as the CO_2 pressure rises from 14 to 20 MPa. In contrast, the permeability damage rate increases significantly, from 13.91% to 38.23%. SEM images (Fig. 5(f)) reveal organic deposits on pore surfaces after high-pressure CO_2 flooding. Flow pathways within the pore network—pores and microfractures—are partially or completely blocked by heavy-component aggregates, which reduces pore connectivity and leads to permeability reduction. Therefore, miscible flooding intensifies deposition-related permeability damage relative to immiscible operations.

Overall, miscible CO_2 flooding in homogeneous cores achieves high recovery (77.08% at 20 MPa) but is accompanied by severe formation damage (15.28% deposition and a 38.23% reduction in permeability). In fractured cores, deposition is lower, however displacement efficiency is reduced, with recovery reaching only 46.04% at 20 MPa. The presence of more than 30% unswept oil in the matrix blocks underscores the need for subsequent mobilization using solvent-type additives to further enhance recovery.

3.4. Effect of TBC on the physical properties of crude oil

Fig. 6 shows the influence of TBC on the physical properties of crude oil under different CO_2 concentrations. Without TBC, both the density and viscosity of the CO_2–oil system decrease as the CO_2 concentration increases (Fig. 6(a) and (b)), reflecting the dilution and swelling effects caused by dissolved CO_2. After the addition of TBC, the density and viscosity are consistently lower than those of the untreated system at the same CO_2 concentration, indicating that TBC further modifies CO_2–oil interactions and improves the fluidity of the CO_2–oil system. In addition, Fig. 6(c) shows that CO_2 solubility increases with CO_2 concentration; at the same CO_2 concentration, the solubility is consistently higher in the presence of TBC than in the untreated system. Fig. 6(d) further shows a larger expansion coefficient after TBC addition, consistent with enhanced CO_2 dissolution and stronger oil swelling.

Overall, the increased CO_2 solubility and swelling, together with the further reduction in density and viscosity after TBC addition, indicate that TBC can improve the fluidity and phase behavior of the CO_2–oil system, which is favorable for flow and displacement during CO_2 flooding.

3.5. Effect of TBC on CO_2 flooding performance

Heavy-component deposition during CO_2 flooding changes pore structures and impairs oil mobility, leading to a significant decline in displacement efficiency (Wei et al., 2021). To mitigate these adverse effects, TBC was injected following CO_2 flooding to enhance recovery and restore permeability. The experimental results at different pressures are shown in Fig. 7.

During the initial CO_2 flooding stage (Fig. 7(a)), recovery increases rapidly with gas injection and gradually stabilizes after breakthrough. The final recovery reaches 39.41%, 68.65%, and 77.08% at 14, 18, and 20 MPa, respectively. After TBC injection, a distinct increase in recovery is observed, particularly at higher pressures. The final recovery increases to 57.34%, 81.95%, and 90.41%, representing incremental improvements of 17.93%, 13.30%, and 13.33%, respectively, as shown in Fig. 7(b). These results indicate that TBC is effective in further mobilizing residual oil after CO_2 flooding under both immiscible and miscible conditions.

The role of TBC, however, appears to differ with flooding condition. At immiscible pressure (14 MPa), where CO_2–oil interaction is relatively limited and deposition is less severe, the recovery improvement is mainly associated with enhanced oil fluidity after TBC treatment. Under miscible conditions (18–20 MPa), where CO_2 extraction and deposition are more pronounced, the substantial incremental recovery suggests that TBC contributes more effectively to the mobilization of deposition-affected residual oil. The stronger response at higher pressures also indicates that the performance of TBC is closely related to the severity of CO_2-induced compositional redistribution and deposition.

3.6. Mobilization mechanism of heavy component by TBC

The pore-scale behavior associated with TBC-induced mobilization of heavy components is shown in Fig. 8(a) and (b). At the initial oil-saturation stage, the NMR T_2 spectrum exhibits a continuous bimodal distribution (Fig. 8(a)). The left peak, associated with small pores, is higher than the right peak for large pores, suggesting abundant small pores and good pore connectivity. After CO_2 flooding at 20 MPa, both peaks decrease markedly, indicating miscible extraction and displacement across pores of different sizes. Magnetic resonance imaging (MRI) profiles show intensified oil signals near the inlet and a high-intensity gas channel along the upper part of the core, indicating preferential deposition of heavy components and early CO_2 breakthrough (Fig. 8(b)). Following TBC injection, the inlet-end deposition weakens, the displacement front becomes more uniform, and both T_2 peaks decrease synchronously, demonstrating simultaneous mobilization of fluids in both large and small pores.

The compositional variations in Fig. 8(c) and (d) further reflect hydrocarbon redistribution during CO_2 flooding and subsequent

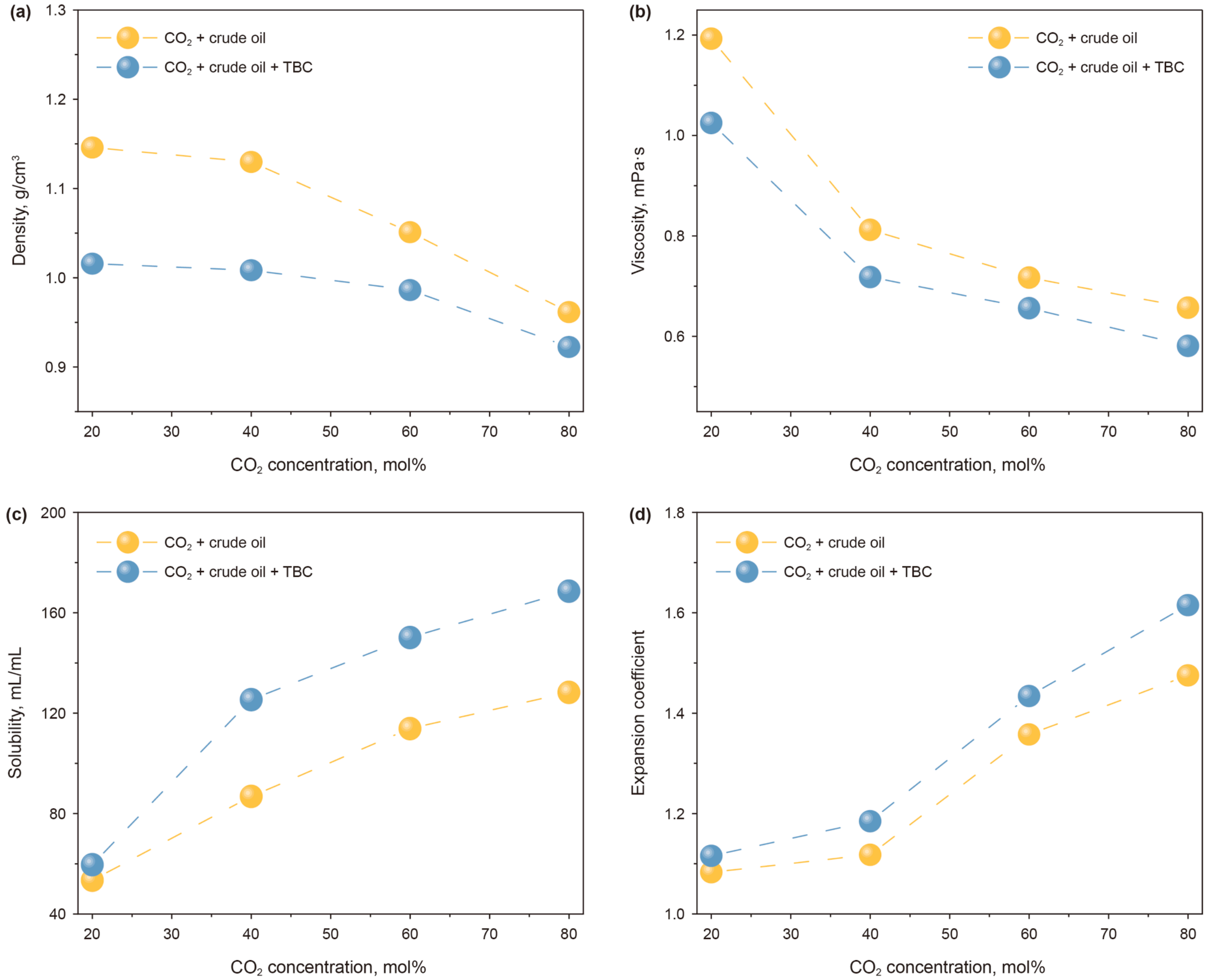

Fig. 6. Effect of TBC on crude–oil physical properties at different CO_2 concentrations: (**a**) density; (**b**) viscosity; (**c**) solubility; (**d**) expansion coefficient.

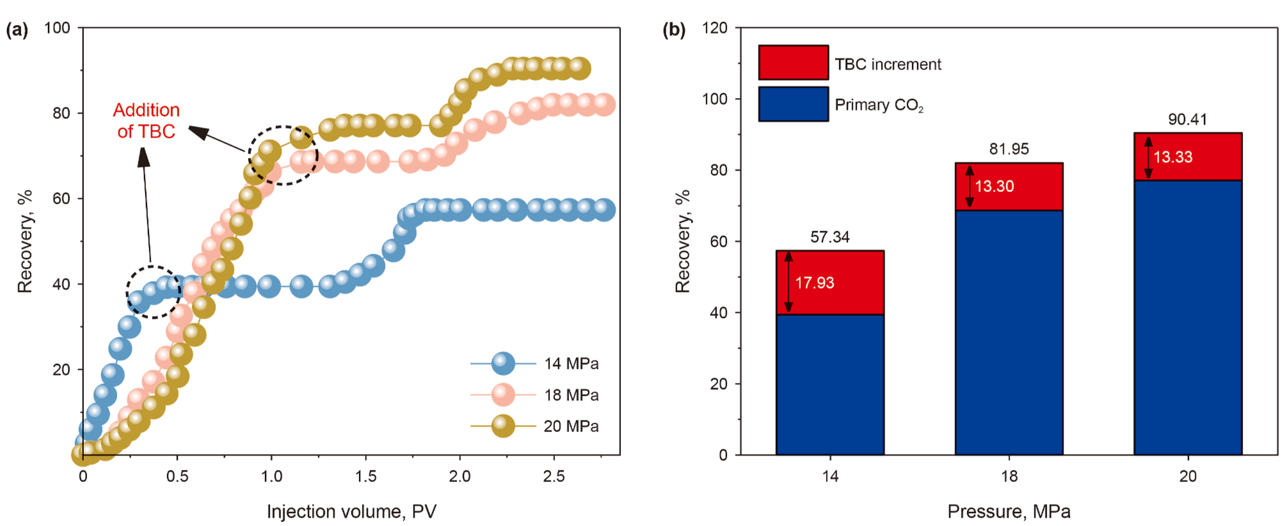

Fig. 7. Effect of TBC on recovery during CO_2 flooding: (**a**) recovery curves at different injection pressures; (**b**) contributions of primary CO_2 flooding and TBC-induced incremental recovery at different pressures.

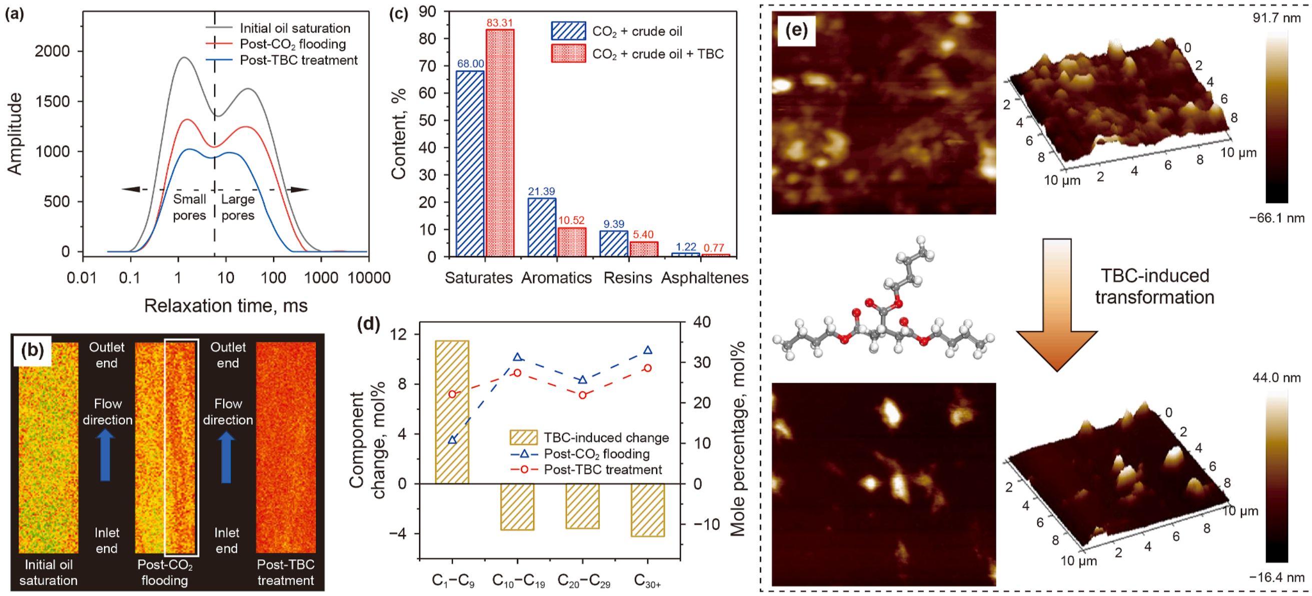

Fig. 8. Multi-scale characterization of TBC-induced heavy-component mobilization: (**a**, **b**) NMR T_2 spectra and MRI fluid-distribution profiles; (**c**, **d**) SARA fractions and carbon number distributions pre- and post-TBC treatment; (**e**) AFM images of heavy-component aggregates before and after TBC treatment.

TBC treatment. After CO_2 flooding, the crude oil retained in the core contains relatively high proportions of aromatics, resins, and asphaltenes, indicating the retention of polar heavy components within the pore network (Fig. 8(c)). With TBC addition, the saturates fraction increases substantially (from 68.00% to 83.31%), while aromatics, resins, and asphaltenes decrease simultaneously. In the carbon number distribution (Fig. 8(d)), the C_1–C_9 fraction increases, whereas the C_{10}–C_{19}, C_{20}–C_{29}, and C_{30+} fractions decrease. These changes are consistent with the mobilization of long-chain and polar heavy components. It is indicated that TBC enhances their dispersion and mobilization within the pore system.

The microscopic morphology and deposition thickness of heavy components before and after TBC treatment were characterized by AFM, as shown in Fig. 8(e). Before TBC treatment, the surface of the deposit was covered with dense columnar aggregates, whereas after TBC treatment, the aggregates became smaller and more dispersed. Multi-region AFM analysis showed that the average thickness of the deposition decreased from 91.7 to 44.0 nm with an error margin of ±0.5 nm after TBC treatment. These morphological changes suggest that TBC substantially reduces interparticle adhe sion and promotes disaggregation of heavy components.

At the molecular level, the observed reduction in aggregate size and deposition thickness after TBC treatment suggests that TBC may improve the dispersion of deposited heavy components (Campen et al., 2020; Zhu et al., 2024). Considering its oxygen-containing functional groups and amphiphilic molecular structure, TBC may enhance the solvation of polar heavy fractions and weaken their aggregation tendency. As illustrated in Fig. 9, TBC may interact with heteroatom-containing sites in asphaltenic and resinous species, thereby reducing intermolecular associations within the aggregates (Horeh et al., 2023; Osei et al., 2024). Overall, these results suggest that TBC promotes the redispersion

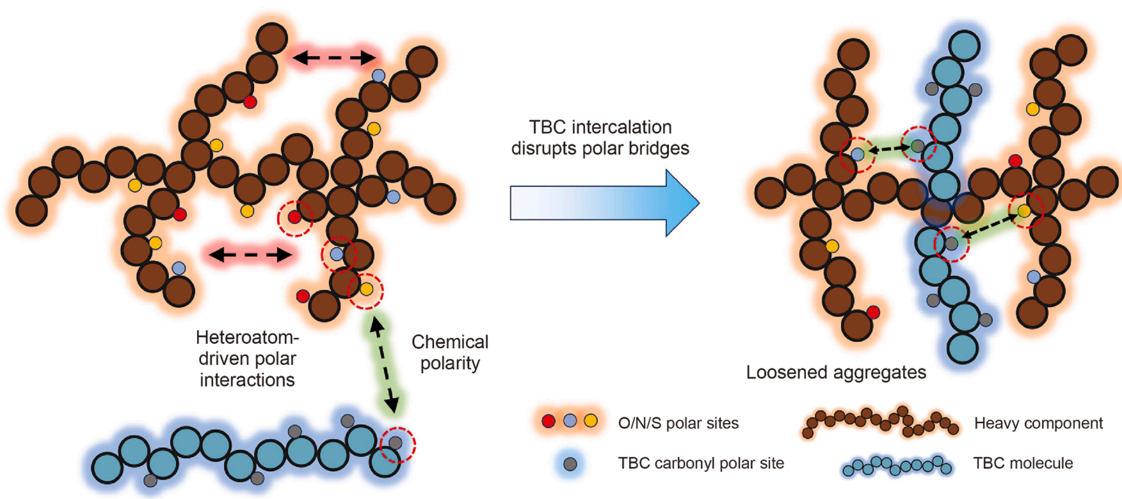

Fig. 9. Molecular mechanism of TBC-assisted disaggregation and mobilization of heavy components.

and remobilization of deposited heavy components, thereby improving pore-scale flow continuity during subsequent CO_2 flooding (Tirjoo et al., 2019).

4. Potential application of TBC

Although miscible CO_2 flooding can significantly improve oil recovery, the experimental results show that it can aggravate heavy-component deposition and permeability damage under strong CO_2–oil interaction. The remaining heavy-component oil after CO_2 flooding is deposition-affected and difficult to remobilize by gas flooding alone. In this work, TBC is more reasonably regarded as a targeted solvent-type additive for post-CO_2-flooding treatment or deposition-damage remediation, rather than a universal additive for all flooding stages. Its potential application value lies in improving pore-scale flow continuity, enhancing the mobility of deposition-affected residual oil, and alleviating flow impairment caused by heavy-component accumulation. From an engineering perspective, TBC would be more reasonably deployed after substantial CO_2 exposure, once deposition-related flow impairment has become evident. Alternating TBC and CO_2 injection may also be considered as a possible strategy, although it still requires further validation. Under carbon-neutrality and CCUS-oriented development scenarios, such a strategy may help balance enhanced oil recovery with the need to maintain injectivity and reduce deposition-related damage. However, its actual effectiveness and economic viability will still depend on reservoir heterogeneity, injection design, and field-scale operating conditions.

5. Conclusions

This study systematically investigated the compositional evolution, asphaltene/resin (heavy-fraction) deposition, and TBC-assisted mobilization behavior of light crude oil during CO_2 flooding. By integrating visual PVT analysis, core-scale displacement experiments, and multi-scale characterization techniques (NMR, SEM, AFM), the following conclusions were drawn.

(1) CO_2–oil interactions under reservoir conditions induce compositional redistribution, characterized by the extraction of light hydrocarbons and the enrichment of heavy fractions in the residual oil. This process promotes deposition of heavy components and causes formation damage. Although miscible CO_2 flooding achieved a high recovery of 77.08% at 20 MPa, it also resulted in permeability damage of up to 38.23%.

(2) TBC improves the physical properties and phase behavior of the CO_2–oil system by suppressing viscosity increase, enhancing CO_2 solubility and oil swelling, and improving CO_2–oil compatibility. As a result, TBC provided an additional 13%–18% recovery beyond CO_2 flooding alone.

(3) Multiscale characterization results suggest that TBC facilitates the redispersion and mobilization of deposited heavy components, thereby improving pore-scale flow continuity and enhancing the recovery of residual oil affected by deposition after CO_2 flooding.

CRediT authorship contribution statement

Zhi-Hao Zhang: Writing – original draft, Data curation. **Ming-Wei Zhao:** Methodology, Conceptualization. **Zhong-Zheng Xu:** Supervision. **Qin-Fang Ding:** Validation. **Yu-Xin Xie:** Writing – review & editing. **Ying-Nan Wang:** Validation. **Yi-Zheng Zhang:** Validation. **Huan Zhang:** Formal analysis. **Xu-Guang Song:** Data curation.

Declaration of competing interest

The authors declare that they have no known competing financial interests or personal relationships that could have appeared to influence the work reported in this paper.

Acknowledgements

The work was supported by the National Science and Technology Major Project on New Types of Oil and Gas Exploration and Development "Innovative Technologies in Oil and Gas Field Geomechanics and Reservoir Stimulation" (2025ZD1401400), “Advanced Waterless Stimulation Technology for High-Stress Reservoirs” (2025ZD1401406), the National Natural Science Foundation of China (U24B2033), and the Science and Technology Major Project of Xinjiang Uygur Autonomous Region (2024A01010-5).

References

Al-Azani, K.H., Abu-Khamsin, S.A., Sultan, A.S., 2020. Solubilities of carbon dioxide in ethyl benzoate and triethyl citrate at high temperatures and pressures. J. Chem. Eng. Data 65 (4), 1857–1868. https://doi.org/10.1021/acs.jced.9b01092.

Al-Azani, K.H., Abu-Khamsin, S.A., Sultan, A.S., 2021. Experimental study of blending CO_2 with triethyl citrate for mitigating gravity override during reservoir flooding. Arab. J. Sci. Eng. 46 (7), 6787–6796. https://doi.org/10.1007/s13369-020-04901-z.

Alizadeh, A., Nakhli, H., Kharrat, R., et al., 2011. An experimental investigation of asphaltene precipitation during natural production of heavy and light oil reservoirs: The role of pressure and temperature. Pet. Sci. Technol. 29 (10), 1054–1065. https://doi.org/10.1080/10916460903530531.

Bao, C., Zheng, C., Xu, Y., et al., 2023. Role of rejuvenator properties in determining the activation effects on aged asphalt based on molecular simulations. J. Clean Prod. 405, 136970. https://doi.org/10.1016/j.jclepro.2023.136970.

Bian, H., Qin, X., Luo, W., et al., 2022. Evolution of hydrate habit and formation properties evolution during hydrate phase transition in fractured-porous medium. Fuel 324, 124436. https://doi.org/10.1016/j.fuel.2022.124436.

Campen, S., Moorhouse, S.J., Wong, J.S.S., 2020. Mechanism of an asphaltene inhibitor in different depositing environments: Influence of colloid stability. J. Pet. Sci. Eng. 184, 106502. https://doi.org/10.1016/j.petrol.2019.106502.

Cao, W., 2023. Exploring the deagglomerating behaviors of selected additives on oxidized asphaltenes using the steered molecular dynamics approach. J. Mol. Liq. 375, 121327. https://doi.org/10.1016/j.molliq.2023.121327.

Cao, W., Li, X., 2022. The rejuvenating potential of plasticizers on oxidatively aged asphalts: Rheological and molecular dynamics perspectives. Polymers 14 (21), 4624. https://doi.org/10.3390/polym14214624.

Chen, J., Jin, X., Li, L., et al., 2023. Construction and performance evaluation of novel compound oil displacement system for enhanced oil recovery. J. Mol. Liq. 387, 122618. https://doi.org/10.1016/j.molliq.2023.122618.

Cheshkova, T.V., Sergun, V.P., Kovalenko, E.Y., et al., 2019. Resins and asphaltenes of light and heavy oils: Their composition and structure. Energy Fuels 33 (9), 7971–7982. https://doi.org/10.1021/acs.energyfuels.9b00285.

Choiri, M., Hamouda, A.A., 2011. Study of CO_2 effect on asphaltene precipitation and compositional simulation of asphaltenic oil reservoir. In: SPE International Conference on Oilfield Chemistry. https://doi.org/10.2118/141329-MS.

Ding, M., Yue, X.A., Zhao, H., et al., 2013. Extraction and its effects on crude oil properties during CO_2 flooding. Energy Sources A: Recovery Util. Environ. Eff. 35 (23), 2233–2241. https://doi.org/10.1080/15567036.2013.816804.

El-Hoshoudy, A.N., Ghanem, A., Desouky, S.M., 2021. Imidazolium-based ionic liquids for asphaltene dispersion; experimental and computational studies. J. Mol. Liq. 324, 114698. https://doi.org/10.1016/j.molliq.2020.114698.

Gao, Y., Tian, W., Li, Y., et al., 2023. Study on compatibility mechanism of plasticizer and asphalt based on molecular dynamics. Mater. Des. 228 (1), 111827. https://doi.org/10.1016/j.matdes.2023.111827.

Guo, J.J., Di, K.X., Zhang, L.H., et al., 2024. Insights into in-situ imbibition behavior of fracturing fluid in propped shale fractures based on nuclear magnetic resonance: A case study from Longmaxi Formation shale, Sichuan Basin, China. Pet. Sci. 21 (1), 410–429. https://doi.org/10.1016/j.petsci.2023.09.023.

Holm, L.W., Josendal, V.A., 1974. Mechanisms of oil displacement by carbon dioxide. J. Pet. Technol. 26 (12), 1427–1438. https://doi.org/10.2118/4736-PA.
Horeh, N.B., Hosseinpour, N., Bahramian, A., 2023. Asphaltene inhibitor performance as a function of the asphaltene molecular/aggregate characteristics: Evaluation by interfacial rheology measurement and bulk methods. Fuel 339, 127420. https://doi.org/10.1016/j.fuel.2023.127420.
Hou, B., He, H., Jia, R., et al., 2019. A novel temperature-tolerant foamed resin for enhanced oil recovery. J. Appl. Polym. Sci. 136 (10), 47161. https://doi.org/10.1002/app.47161.
Hu, Y.L., Hao, M.Q., Chen, G.L., et al., 2019. Technologies and practice of CO_2 flooding and sequestration in China. Petroleum Explor. Dev. 46 (4), 753–766. https://doi.org/10.1016/S1876-3804(19)60233-8.
Huang, X., Zhang, Y., He, M., et al., 2022. Asphaltene precipitation and reservoir damage characteristics of CO_2 flooding in different microscopic structure types in tight light oil reservoirs. Fuel 312, 122943. https://doi.org/10.1016/j.fuel.2021.122943.
Jia, H., Wu, H., Wei, X., et al., 2020. Investigation on the effects of AlOOH nanoparticles on sodium dodecylbenzenesulfonate stabilized o/w emulsion stability for EOR. Colloids Surf. A Physicochem. Eng. Asp. 603, 125278. https://doi.org/10.1016/j.colsurfa.2020.125278.
Jiang, K., Ashworth, P., 2021. The development of carbon capture utilization and storage (CCUS) research in China: A bibliometric perspective. Renew. Sustain. Energy Rev. 138, 110521. https://doi.org/10.1016/j.rser.2020.110521.
Ke, C.Y., Sun, W.J., Li, Y.B., et al., 2018. Polymer-assisted microbial-enhanced oil recovery. Energy Fuels 32 (5), 5885–5892. https://doi.org/10.1021/acs.energyfuels.8b00812.
Kumar, N., Sampaio, M.A., Ojha, K., et al., 2022. Fundamental aspects, mechanisms and emerging possibilities of CO_2 miscible flooding in enhanced oil recovery: A review. Fuel 330, 125633. https://doi.org/10.1016/j.fuel.2022.125633.
Lashkarbolooki, M., Ayatollahi, S., 2018. Experimental investigation on CO_2-light crude oil interfacial and swelling behavior. Chin. J. Chem. Eng. 26 (2), 373–379. https://doi.org/10.1016/j.cjche.2017.07.010.
Li, H.B., Yang, Z.M., Li, R.S., et al., 2021a. Mechanism of CO_2 enhanced oil recovery in shale reservoirs. Pet. Sci. 18 (6), 1788–1796. https://doi.org/10.1016/j.petsci.2021.09.040.
Li, R.T., Liao, X.W., Zou, J.D., et al., 2021b. Asphaltene deposition during CO_2 flooding in ultralow permeability reservoirs: A case study from Changqing oil field. Geofluids, 6626114. https://doi.org/10.1155/2021/6626114.
Li, S., Wang, Q., Zhang, K., et al., 2020. Monitoring of CO_2 and CO_2 oil-based foam flooding processes in fractured low-permeability cores using nuclear magnetic resonance (NMR). Fuel 263, 116648. https://doi.org/10.1016/j.fuel.2019.116648.
Martin, D.F., Taber, J.J., 1992. Carbon dioxide flooding. J. Pet. Technol. 44 (4), 396–400. https://doi.org/10.2118/23564-PA.
Mehrabianfar, P., Bahraminejad, H., Manshad, A.K., 2021. An introductory investigation of a polymeric surfactant from a new natural source in chemical enhanced oil recovery (CEOR). J. Pet. Sci. Eng. 198, 108172. https://doi.org/10.1016/j.petrol.2020.108172.
Mousavi, M., Abdollahi, T., Pahlavan, F., et al., 2016. The influence of asphaltene-resin molecular interactions on the colloidal stability of crude oil. Fuel 183, 262–271. https://doi.org/10.1016/j.fuel.2016.06.100.
Osei, F.B., Twum, K., Surapaneni, S., et al., 2024. A resorcinarene-based crude oil asphaltene dispersant. Fuel 375, 132428. https://doi.org/10.1016/j.fuel.2024.132428.
Rezk, M.G., Foroozesh, J., 2019. Phase behavior and fluid interactions of a CO_2-light oil system at high pressures and temperatures. Heliyon 5 (7), e02057. https://doi.org/10.1016/j.heliyon.2019.e02057.
Sarma, H.K., 2003. Can we ignore asphaltene in a gas injection project for light-oils?. In: SPE International Improved Oil Recovery Conference. https://doi.org/10.2118/84877-MS.
Seyyedsar, S.M., Farzaneh, S.A., Sohrabi, M., 2016. Experimental investigation of tertiary CO_2 injection for enhanced heavy oil recovery. J. Nat. Gas Sci. Eng. 34, 1205–1214. https://doi.org/10.1016/j.jngse.2016.08.020.
Shen, Z., Sheng, J.J., 2018. Experimental and numerical study of permeability reduction caused by asphaltene precipitation and deposition during CO_2 huff and puff injection in Eagle Ford shale. Fuel 211, 432–445. https://doi.org/10.1016/j.fuel.2017.09.047.
Tan, J., Wang, Z., Chen, S., et al., 2023. Progress and outlook of supercritical CO_2-heavy oil viscosity reduction technology: A minireview. Energy Fuels 37 (16), 11567–11583. https://doi.org/10.1021/acs.energyfuels.3c01387.
Tirjoo, A., Bayati, B., Rezaei, H., et al., 2019. Molecular dynamics simulations of asphaltene aggregation under different conditions. J. Pet. Sci. Eng. 177, 392–402. https://doi.org/10.1016/j.petrol.2019.02.041.
Wang, Y., Ge, J., Zhang, W., et al., 2016. Surface property and enhanced oil recovery study of foam aqueous dispersions comprised of surfactants organic acids nanoparticles. RSC Adv. 6 (114), 113478–113486. https://doi.org/10.1039/C6RA22988C.
Wang, Y., Han, X., Li, J., et al., 2023. Review on oil displacement technologies of enhanced oil recovery: State-of-the-art and outlook. Energy Fuels 37 (4), 2539–2568. https://doi.org/10.1021/acs.energyfuels.2c03625.
Wei, B., Zhang, X., Liu, J., et al., 2020. Supercritical CO_2-EOR in an asphaltenic tight sandstone formation and the changes of rock petrophysical properties induced by asphaltene precipitation. J. Pet. Sci. Eng. 184, 106515. https://doi.org/10.1016/j.petrol.2019.106515.
Wei, J., Zhou, J., Li, J., et al., 2021. Experimental study on oil recovery mechanism of CO_2 associated enhancing oil recovery methods in low permeability reservoirs. J. Pet. Sci. Eng. 197, 108047. https://doi.org/10.1016/j.petrol.2020.108047.
Xue, F., Yang, L., Li, J., et al., 2024. Effect of tributyl citrate as a cosolvent on the phase behavior of crude oil during CO_2 injection process. Energies 17 (2), 410. https://doi.org/10.3390/en17020410.
Yang, Z., Wu, W., Dong, Z., et al., 2019. Reducing the minimum miscibility pressure of CO_2 and crude oil using alcohols. Colloids Surf. A Physicochem. Eng. Asp. 568, 105–112. https://doi.org/10.1016/j.colsurfa.2019.02.004.
Yu, T., Li, Q., Hu, H., et al., 2022. Residual oil retention and stripping mechanism of hydrophilic pore surfaces during CO_2 and N_2 combined gas flooding. J. Pet. Sci. Eng. 218, 110989. https://doi.org/10.1016/j.petrol.2022.110989.
Yuan, R., Gao, L., Liu, J., et al., 2024. Effect of hydrophobic alkyl chains on the plasticization properties of citrate: Experiments and MD simulation. Eur. Polym. J. 203, 112644. https://doi.org/10.1016/j.eurpolymj.2023.112644.
Yuan, Z., Liu, Q., Luo, B., et al., 2018. Thermodynamic analysis of different oil flooded compression enhanced vapor injection cycles. Energy 154, 553–560. https://doi.org/10.1016/j.energy.2018.04.182.
Zhang, X., Su, Y., Li, L., et al., 2022. Microscopic remaining oil initiation mechanism and formation damage of CO_2 injection after waterflooding in deep reservoirs. Energy 248, 123649. https://doi.org/10.1016/j.energy.2022.123649.
Zhao, X., Yang, L., Li, J., et al., 2025. Recovering residual heavy oil after CO_2 flooding by middle-phase microemulsion. Ind. Eng. Chem. Res. 64 (9), 4725–4735. https://doi.org/10.1021/acs.iecr.4c04463.
Zhong, X., Chen, J., An, R., et al., 2021. A state-of-the-art review of nanoparticle applications with a focus on heavy oil viscosity reduction. J. Mol. Liq. 344, 117845. https://doi.org/10.1016/j.molliq.2021.117845.
Zhu, B., Li, Z., Han, T., et al., 2024. Molecular insights into the dispersibility of asphaltene and crude oil rheological properties under the effect of multi-alkylated aromatic amides. Chem. Eng. Sci. 285, 119548. https://doi.org/10.1016/j.ces.2023.119548.
Zuo, M., Chen, H., Qi, X., et al., 2023. Effects of CO_2 injection volume and formation of in-situ new phase on oil phase behavior during CO_2 injection for enhanced oil recovery (EOR) in tight oil reservoirs. Chem. Eng. J. 452, 139454. https://doi.org/10.1016/j.cej.2022.139454.